Available online at www.sciencedirect.com
SCIENCE DIRECT
Polymer 47 (2006) 5657–5668
polymer
www.elsevier.com/locate/polymer

Effects of high molecular weight species on shear-induced orientation and crystallization of isotactic polypropylene

Rajesh H. Somani, Ling Yang, Benjamin S. Hsiao *

Department of Chemistry, State University of New York, Stony Brook, NY 11794-3400, USA

Received 23 October 2004; accepted 10 December 2004
Available online 16 May 2006

This paper is dedicated to Prof. David C. Bassett on the occasion of his retirement.

Abstract

In situ rheo-SAXS (small-angle X-ray scattering) and—rheo-WAXD (wide-angle X-ray diffraction) techniques were used to investigate the role of high molecular weight species on the evolution of oriented microstructure in isotactic polypropylene (*i*PP) melt under shear flow. The two *i*PP samples, designated as PP-A and PP-B, respectively, had the same number-average (M_n) but different weight-average (M_w) and *Z*-average (M_z) molecular weights. Molecular weight distribution (MWD) of PP-A and PP-B was such that for MW $< 10^5$ the MWD curves overlapped; whereas in the high MW tail region, the amount of high molecular weight species was higher in PP-B than PP-A. Both samples were subjected to an identical shear condition (rate = 60 s^{-1}, duration = 5 s, $T = 155$ °C). In situ 2D SAXS and WAXD images allowed the tracking of shear-induced oriented structures in the melt. It was found that the shish structures evolved much earlier, and the degree of crystal orientation and oriented crystal fractions were higher in PP-B than PP-A. Moreover, PP-B exhibited faster crystallization kinetics than PP-A. These results, along with the predictions of double reptation models of chain motion and experimental studies of chain conformation dynamics in dilute solutions under flow, suggest the following: When a polymer melt that consists of entangled chains of different lengths is deformed, the chain segments aligned with the flow eigenvector can undergo the abrupt *coil-stretch*-like transition, while other segments would remain in the coiled state. Since, flow-induced orientation decays much more slowly for long chains than for short chains, oriented high molecular weight species play a prominent role in formation of the stretched sections, where shish originates. Our experimental results are strong evidence of the hypothesis that even a small increase in the concentration of high molecular weight species causes a significant increase in the the formation, stability and concentration of the flow-induced oriented microstructure.

Keywords: Isotactic polypropylene; Crystallization; Shear flow

1. Introduction

Polymer melts under flow exhibit many important macroscopic effects, including flow-dependent viscosity, higher normal stresses, enhanced nucleation and crystallization rate and shish–kebab morphology. These are related to the flow-induced structural changes from liquid to solid states. The extent of these changes depends upon the type and intensity of the flow field [1]. In general, polymer crystallization evolves through formation of stable nuclei; which are thought to consist of a certain minimum number of aligned chain segments [2–5]. The nucleation process is dictated by stochastic events such as Brownian motion of chain segments and, surprisingly, is very fast, on the order of nanoseconds [6]. In flow, molecules orient and/or stretch. Clearly, the degree of molecular orientation and/or extension affects their ability to organize, align and form stable primary nuclei. These early stage nucleation events lead to formation of a scaffold of nuclei, which are also termed the oriented microstructures [7–12]. Upon crystallization, it manifests into crystals with varying degrees of orientation, and the final polymer morphology exhibits a distribution of the oriented and unoriented crystals. It should be emphasized that these structures evolve in the polymer melt at very early stages of crystallization. Clearly, control of the initial nuclei landscape is the key to manipulating the final morphology and properties [13–25]. For this, knowledge of its characteristics; i.e. density (number of nuclei/volume) and nature of nuclei (shish or point-like) and their degree of orientation (with respect to the flow direction), is essential. In addition to the flow parameters, polymer structural properties such as

* Corresponding author. Tel.: +1 631 632 7793; fax: +1 631 632 6518.
E-mail address: bhsiao@notes.cc.sunysb.edu (B.S. Hsiao).

0032-3861/$ - see front matter © 2006 Elsevier Ltd. All rights reserved.
doi:10.1016/j.polymer.2004.12.066

molecular weight (MW) and molecular weight distribution (MWD) obviously affect, both qualitatively and quantitatively, the characteristics of the flow-induced oriented microstructures, which is the subject of this paper.

Extensive studies of the effects of MW and MWD on polymer crystallization rate and morphology can be found in the literature. For example, Monasse and coworkers [26] performed fiber pullout experiments at 125–130 °C using three *i*PP polymers that differ in MW. They found that the crystallization rate exponentially increased with MW. Their study included three different polypropylenes: Ziegler-Natta based and Metallocene based homopolymers, as well as ethylene–propylene copolymers. The growth rate enhancement under shear at 126 °C was found to be governed by MW, especially the weight-average molecular weight (M_w). A rheological study of three *i*PP polymers with differing MW and MWD at 138–140 °C by Vleeshouwers and Meijer [27] showed that the high molecular weight tail enhanced crystallization after shear. The results of short-term shear experiments of Jerschow and Janeschitz-Kriegl [28] with *i*PP at low degrees of showed that long polymer molecules were predominantly responsible for the formation of highly oriented surface layers due to shear. Bove and Nobile [29] reported in situ optical analysis of step shear experiments at 86 and 95 °C performed in a Linkam shear stage with two poly(1-butene) samples having different M_w and *z*-average molecular weights (M_z). The higher molecular weight sample showed shorter induction times and enhanced nucleation density. They concluded that M_w and M_z are the most effective averages in the flow-induced crystallization. Recently, Acierno, et al. [30] carried out rheological and rheo-optical shear flow experiments on a sequence of isotactic poly(1-butene) of different M_w (116–398 k) at a temperature of 103 °C. They found that, while the quiescent crystallization was essentially M_w-independent, an increase of M_w resulted in larger nucleation and crystallization rates at a given shear rate. Also, the optical micrographs of crystallizing polymer revealed that a transition from an isotropic to a rod-like morphology occurred at high values of flow intensity, which was characterized by the Weissenberg number, W_i = shear rate × longest relaxation time. The longest relaxation time implicitly contains information on the polymer molecular weight.

From the physical viewpoint, basic mechanisms of the molecular weight effects in flow-induced crystallization are relatively well understood. For linear polymers, relaxation time scales as 3.4 power of the molecular weight. After cessation of flow, long (or high MW) chains can remain oriented for longer time than short (or low MW) chains. Thus, in polydisperse polymers, the flow effects on the crystallization kinetics and morphology can be related to the presence of a long tail of high MW chains. However, the role of long chains in the formation of oriented structures at the early stages of crystallization is not entirely clear. In this regard, the experimental temperature (T) or degree of supercooling (with reference to the melting point of polymer, T_m), $\Delta T = T_m - T$, plays a key role because of the following reasons. At high ΔT, crystallization rate is high, which is further enhanced in flow, and both the oriented and unoriented crystals can simultaneously crystallize. The unoriented crystals can overwhelm the resultant crystalline phase microstructure if ΔT is too large, such that the observation of the characteristic features of oriented structures would become difficult. (Note that most of the previous studies were performed at large ΔT). At small ΔT, it is easier to discriminate between the oriented and unoriented structures. However, suitable techniques with high sensitivity are required for the detection. In these aspects, in situ rheo-SAXS (small-angle X-ray scattering) and -WAXD (wide-angle X-ray diffraction) techniques using high intensity synchrotron X-rays have unique advantages. Synchrotron X-rays provide high sensitivity and allow detection of the oriented structures at the early stages of their evolution. We have successfully used these techniques for characterizing the flow-induced oriented structures in many polymer systems including *i*PP [31–34], long chain branched *i*PP [35], a blend of *i*PP and atactic-PP [36], polyethylene (PE), and blends of low and high molecular weight PE [37]. In this study, a temperature of 155 °C was selected for rheo-SAXS and -WAXD experiments, which corresponds to ΔT of about 8 °C for the chosen *i*PP samples. The real time 2D SAXS and WAXD images allowed the observation of the subtle differences in the oriented microstructures as they evolve in the sheared melt.

2. Experimental

Two experimental isotactic samples, PP-A and PP-B, made by the Ziegler-Natta method were chosen for this study. Their molecular weights (number-averaged molecular weight, M_n, weight-averaged molecular weight, M_w, and *z*-averaged molecular weight, M_z) and melt index are presented in Table 1, where M_w and M_z were higher for PP-B than PP-A, and M_n was about the same for both samples. Fig. 1(a) compares the molecular weight distribution (MWD) curves for PP-A and PP-B, obtained by gel permeation chromatography (GPC). It was found that MWD curves of both polymers overlapped in the low molecular weight region ($M < 10^5$). A magnified view of the high molecular weight tail region is illustrated in Fig. 1(b), which showed that the amount of the high molecular weight species was slightly higher in PP-B than in PP-A.

A Linkam CSS-450 high temperature shearing stage modified for in situ X-ray scattering/diffraction studies was used for rheo-SAXS and -WAXD experiments. Details of the shear stage, as well as the experimental procedure, were given in previous publications [31–32]. Typically, a pressed polymer ring, OD = 20 mm, ID = 10 mm and thickness = 0.5–1.0 mm, was mounted between the two parallel plates (X-ray windows) of the shear stage. Prior to shear, the sample was subjected to a

Table 1
Molecular weights (M_n, M_w and M_z) and melt index of PP-A and PP-B

Sample	M_n (g/g mol)	M_w (g/g mol)	M_z (g/g mol)	Melt index
PP-A	46,600	263,900	730,700	7
PP-B	46,200	30,1800	100,4000	4.6

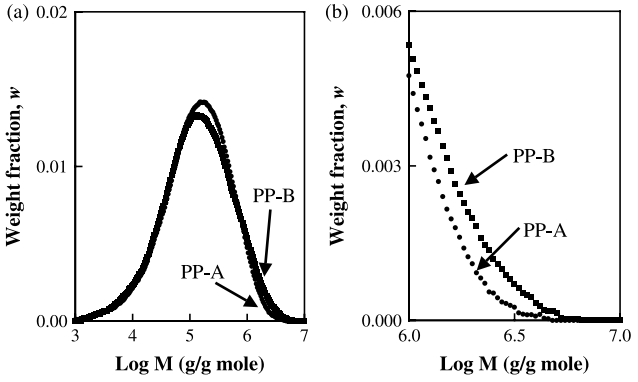

Fig. 1. (a) Comparison of molecular weight distribution (MWD) curves of PP-A and PP-B obtained from GPC. (b) Magnified view of high molecular weight tail region of PP-A and PP-B.

thermal treatment in order to ensure that the polymer melt was free of any memory effects associated with clusters, crystal aggregates and molecular conformation. The temperature protocol for shear experiments was as follows.

1. Heat the sample from room temperature to 200 °C at a rate of 30 °C/min.
2. Hold the temperature at 200 °C for 5 min.
3. Cool at 30 °C/min down to 155 °C.
4. Hold the temperature at 155 °C for 30 min.
5. Cool to room temperature.

The X-ray measurements were carried out in the X27C beamline at the National Synchrotron Light Source (NSLS), Brookhaven National Laboratory (BNL). The wavelength, λ, of X-ray beam was 1.366 Å and 1.371 Å for SAXS and WAXD experiments respectively. A 2D MARCCD detector (MARUSA) was employed for the detection of 2D SAXS and WAXD patterns. The detector resolution was set at 1024 × 1024 pixels (pixel size = 158 μm). X-ray patterns of the standard samples: silver behenate and Al_2O_3, were used for calibration of sample to detector distances for SAXS (1729 mm) and WAXD (111 mm), respectively. One X-ray pattern of the amorphous melt was collected immediately after the temperature reached 155 °C, before shear. Subsequently, the polymer melt was subjected to a step-shear (shear rate = 60 s^{-1}, duration = 5 s). 2D SAXS and WAXD patterns were collected continuously after cessation of shear. One hundred and twenty images, four per minute, were collected in a single run. At the end of the isothermal step, the sample was cooled to room temperature. One X-ray pattern of the sheared sample was also collected at room temperature. All X-ray data were corrected for background (air and instrument) scattering before analysis.

3. Results

3.1. Rheo-SAXS

3.1.1. In situ SAXS images at high temperature

Fig. 2 shows 2D rheo-SAXS patterns of PP-A and PP-B samples before shear and at selected times after cessation of shear. The flow direction is vertical and is considered the same as the fiber axis. The pattern before shear (at $t = 0$) exhibited a weak diffused scattering ring, indicating that the melt was isotropic without any detectable structures and/or preferred orientation. This confirmed that the thermal treatment was effective in erasing prior memory effects. Typically, the equatorial streak in SAXS pattern is attributed to the formation of oriented structures or shish, oriented parallel to the flow direction; meridional maxima are attributed to the layer-like oriented structures or kebabs, oriented perpendicular to the flow direction. SAXS patterns of PP-A and PP-B in Fig. 2 showed, qualitatively, how the imposed shear affected the nature of oriented microstructures as they evolved in the sheared melt. A weak equatorial streak was observed in the pattern of PP-B at $t = 0.5$ min, while the corresponding pattern of PP-A did not show any equatorial scattering. Clearly, the shish structure evolved earlier in PP-B than PP-A. As the shish in the polymer melt must have originated from the clusters of aligned chain segments, the shorter time of their evolution in PP-B can be related to the higher amount of the MW species in the distribution. The kebabs developed after the formation of shish. The scattered intensity of the equatorial streaks and

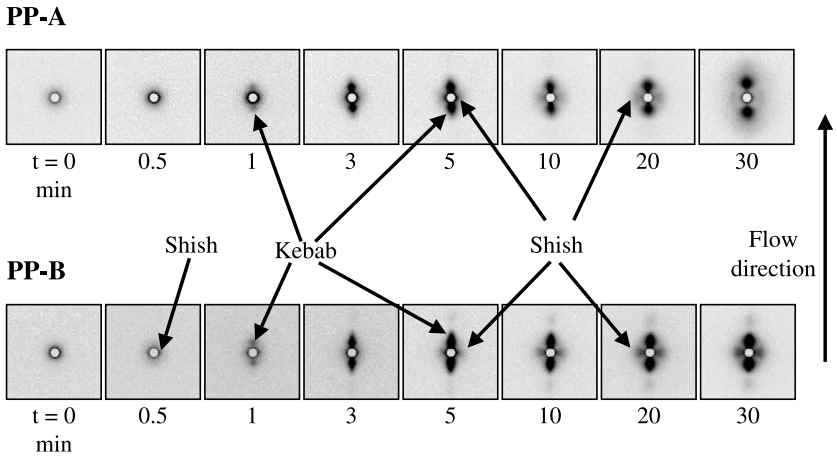

Fig. 2. 2D SAXS images of PP-A and PP-B at selected times after shear (shear rate = 60 s^{-1}, duration = 5 s and $T = 155$ °C).

meridional maxima (indicated by arrows in Fig. 2) increased with time for both polymers, indicating that both shish and kebab contents increase with crystallization time. It is interesting to note that the scattering patterns at the late stages of crystallization for both PP-A and PP-B samples exhibited a cross-like equatorial streak feature, which can be attributed to relaxation of chains, resulting in tilting of the shish structure. The misorientation angle between the cross-like streaks was found to increase with time, which is consistent with the relaxation process. In addition, SAXS patterns at the later stages ($t > 5$ min) showed diffused scattering, superimposed on the oriented features. Quantitative calculations of scattering due to the oriented and unoriented scatterers will be presented in the later section.

3.1.2. SAXS images at room temperature

Fig. 3 shows SAXS patterns obtained after cooling the sheared melt to room temperature (the melt was cooled at the end of the isothermal step; i.e. 30 min after shear). As expected, these patterns exhibited strong total scattered intensity due to the increase in crystallinity. SAXS patterns clearly showed overlaps of (1) diffused scattering (unoriented crystals), (2) equatorial streaks (cross-like due to misoriented shish), and (3) meridional maxima (kebabs). During the cooling step, obviously, all crystallizable species in the polymer melt attempt to crystallize, within the scaffold of the crystallization precursor structure formed at high temperatures. The room temperature pattern clearly resembles the pattern formed at high temperatures, suggesting that the precursor structure dictates the final morphology. It is expected that the initially formed crystals, both oriented and unoriented, grow as well as become more perfect; i.e. the chain segments within the crystals reorganize and align, which increases the electron density contrast, and thus the SAXS intensity. In addition, new crystals can nucleate and grow. Interestingly, these patterns also showed higher order scattering peaks (indicated by arrows in Fig. 3), indicating that the oriented lamellae stacks (kebabs) are well correlated; i.e the average spacing between the layers becomes quite uniform.

3.2. Rheo-WAXD

In WAXD patterns obtained at a wavelength of 1.371 Å, the monoclinic α-crystalline form of *i*PP reflections could be indexed as follows: (110) at $2\theta = 12.6°$, (040) at 15.1°, (130) at 16.6°, (111) at 18.9°, and (−131) at 19.5°, where (110), (040) and (130) reflections were seen on the equator and (111) and (−131) reflections were seen off the meridian axis. In Fig. 4, it is seen that the WAXD image of PP-B collected at time = 1 min after shear exhibited a well-oriented diffraction pattern with strong (110), (040) and (130) reflections on the equator. This suggests that the crystals, formed in the early stage after shear, were very well oriented in the flow direction. The crystals formed at the later stages were less ordered due to the chain relaxation, which is consistent with the observation of the SAXS evolution. In addition, the azimuthal breadths of the crystal reflections were found to be narrower with the increase in the degree of crystal orientation. The azimuthal breadth of the (110) reflection, the strongest among all *i*PP reflections, was used as a marker to estimate the degree of orientation of the 'parent' lamellae or kebabs.

3.2.1. In situ WAXD images at high temperature

Fig. 4 shows rheo-WAXD patterns of the two samples before shear and at selected times after shear. It was seen that, at about 0.5 min after shear, equatorial arcs of (110), (040) and (130) reflections were detected in the WAXD pattern of PP-B, while the corresponding pattern of PP-A did not show any crystal reflections. Clearly, the oriented 'parent' lamellae or kebabs were formed at 0.5 min in the sheared melt of PP-B, while there was no evidence of crystallization in the sheared melt of PP-A during the same time frame. At about 1 min after shear, equatorial arcs of (110), (040) and (130) reflections were detected in the WAXD pattern of PP-A. Subsequently, the intensities of crystal reflections increased with time for both samples as expected. In addition, the patterns at the later stages showed off-meridian arcs of (111) and (−131) reflections. These reflections were detected later because their relative intensity was lower than the other crystal reflections. The patterns at $t > 5$ min, for both polymers, showed evolution of

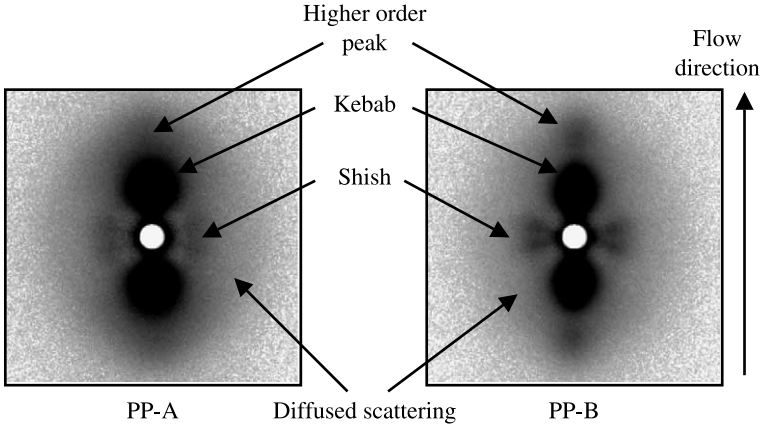

Fig. 3. 2D SAXS images of sheared PP-A and PP-B at room temperature. Note that sheared melt was kept at 155 °C for 30 min after cessation of shear, and then cooled to room temperature.

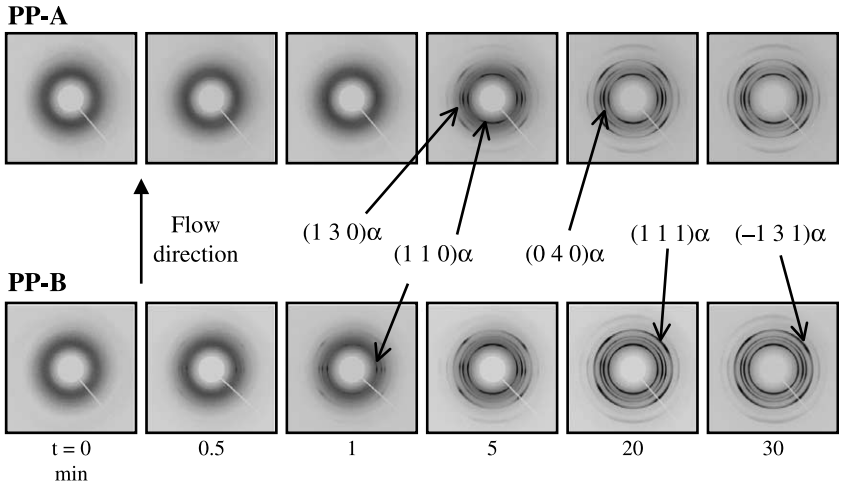

Fig. 4. 2D WAXD images of PP-A and PP-B at selected times after shear (shear rate = 60 s^{-1}, duration = 5 s and T = 155 °C.

rings of uniform intensity overlapping with the equatorial and off-meridional arcs. This is due to the formation of unoriented crystals at the later stages. Qualitatively, the degree of crystal orientation appeared to be higher in PP-B than PP-A. These observations are in according with the corresponding SAXS results (Fig. 2). Results from the quantitative analysis will be presented in later sections.

3.2.2. WAXD images at room temperature

Fig. 5 shows WAXD patterns obtained after cooling the sheared melt to room temperature. As before, the sheared melt was cooled at the end of the isothermal step; i.e. 30 min after shear. It was seen that the intensities of crystal reflections, both arcs and rings, were substantially increased in room temperature images due to the increase in the crystal volume fractions upon cooling. These results were consistent with the SAXS results, and can be attributed to (1) perfection and growth of initially formed crystals, and (2) simultaneous nucleation and growth of new crystals. WAXD patterns also showed higher order crystal reflections, indicated by the arrows in Fig. 5, which again was indicative of a certain degree of perfection in the alignment of chain segments within the oriented lamellae or kebabs.

3.3. Analysis of rheo-SAXS and -WAXD data

3.3.1. Oriented fraction

The total integrated SAXS intensity can be represented as follows

$$I_{\text{total}}[s,\phi] = I_{\text{unoriented}}[s] + I_{\text{oriented}}[s,\phi] \quad (1)$$

where, $s = 2\sin\theta/\lambda$ is the scattering vector, 2θ is the scattering angle, and ϕ is the azimuthal angle. $I_{\text{unoriented}}$ is azimuthal independent (a function of s only), while I_{oriented} is azimuthal dependent (a function of s and ϕ). An image–image subtraction procedure, the Halo method [38], was used to deconvolute the total scattering into contributions due to the oriented and unoriented structures. For example, Fig. 6(a) shows 2D, as acquired total scattering pattern (of PP-B 30 min after shear), and contributions due to the oriented and unoriented parts obtained after deconvolution. Numerical values of the corresponding integrated intensities were obtained from these

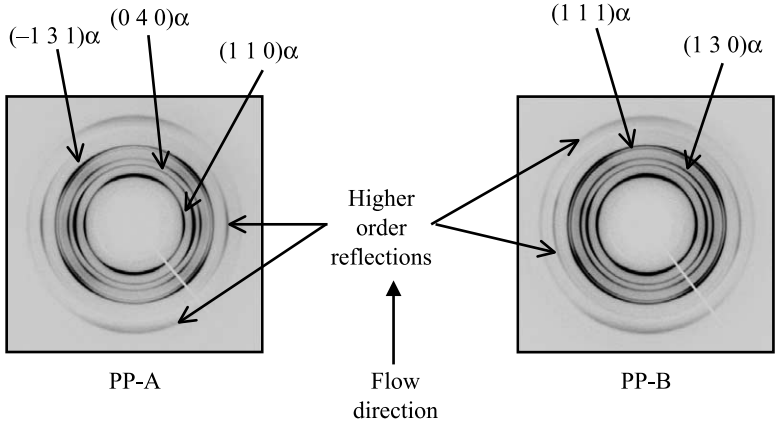

Fig. 5. 2D WAXD images of sheared PP-A and PP-B at room temperature. Note that sheared melt was kept at 155 °C for 30 min after cessation of shear, and then cooled to room temperature.

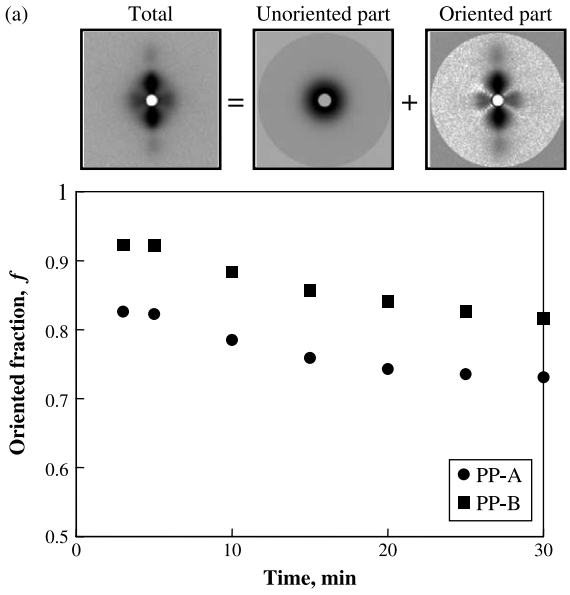

Fig. 6. (a) Total SAXS intensity pattern of sheared PP-B sample and contributions due to the oriented and unoriented part obtained after deconvolution by the Halo method. (b) Oriented fraction, f, as a function of time after shear for PP-A and PP-B (shear rate = 60 s^{-1}, duration = 5 s and T = 155 °C).

2D patterns. Oriented fraction, f, is defined as the ratio of integrated intensity due to the oriented structures and total intensity. Fig. 6(b) shows the calculated f values as a function of time for the two samples. In both samples, f was high in the beginning; immediately after shear, it decreased and appeared to reach a plateau value at later times. This observation can be explained as follows. In the beginning, a short time after shear, the polymer melt primarily consisted of the oriented crystals and its contribution to the total intensity was significantly higher than the contribution due to the unoriented crystals. As a result, high values of f were obtained. Later, the unoriented crystals evolved and grew, increasing its contribution to the total intensity and the relative contribution due to the oriented crystals decrease. Hence, f decreased with time after shear. Fig. 6(b) shows that f is higher for PP-B than PP-A. Similar analysis of the SAXS patterns at room temperature (Fig. 3) gives f values for the final crystallized polymer. The calculated value of f was higher for fully crystallized PP-B (0.77) than PP-A (0.7) at room temperature. These effects could only be attributed to the higher amount of high molecular weight species in PP-B compared to that in PP-A.

3.3.2. Lamellae spacing

Long spacing (or long period) between the kebabs, $L = 2\pi/s_{max}$, was estimated from the position of the intensity maxima along the meridian in the SAXS patterns. Fig. 7 shows time evolution of Lorentz corrected meridional intensity profiles for the two samples. Fig. 8 illustrates the value of long spacing as a function of time. At early times, L was found to be about 44 and 46 nm for PP-A and PP-B, respectively. Later, it decreased and appeared to reach a plateau value (the L value at 30 min after shear was about 35 and 39 nm for PP-A and PP-B, respectively). The L value of PP-A was consistently smaller than that of PP-B, where the decreasing trends were similar in both samples. Generally, the long period value depends on the degree of supercooling, ΔT, under isothermal crystallization. As the melting point for both PP-A and PP-B samples is the same and their molecular distributions are very close, the slightly larger long period value in PP-B than PP-A (by 2–5 nm) is somewhat unexpected. This behavior must be related to the greater amount of the high molecular weight species in PP-B, which can form a larger dimension of shish under flow and result in a slightly less dense kebab formation on the shish. The decreasing trend in L suggests the following. The initially formed shish–kebab structures have a loosely packed lamellar structure and hence a high value of L. This is because at the early stages of kebab formation, the arrangement of chain segments may not be as in a perfect folded chain lamellae crystal. During the growth phase, lamellae chain segments can reorganize, admittedly to a small extent, which would affect L. Also, new kebabs can nucleate at a different location along the shish. These events would lead to the decrease in L at the early stages before reaching a plateau value.

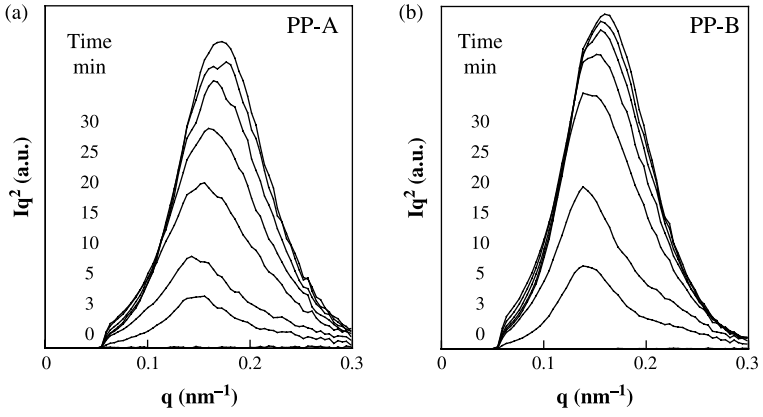

Fig. 7. Lorentz corrected SAXS intensity profiles taken along the meridian as a function of time after shear for PP-A and PP-B (shear rate = 60 s^{-1}, duration = 5 s and T = 155 °C). The long period or the spacing between adjacent lamellae was determined from the position of maxima in these profiles.

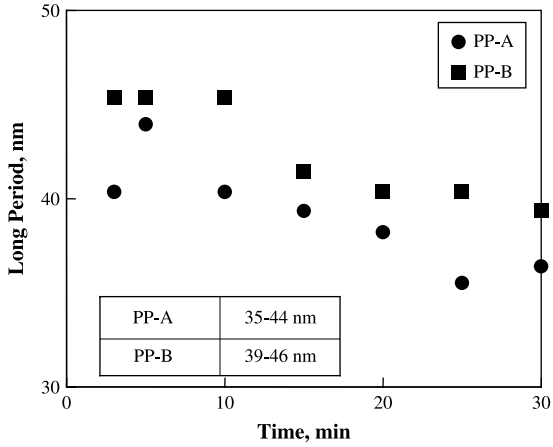

Fig. 8. Time evolution of long period after shear for PP-A and PP-B (shear rate = 60 s^{-1}, duration = 5 s and T = 155 °C).

Fig. 9 shows the Lorentz corrected intensity profiles along the meridian and the calculated values of L for PP-A and PP-B after cooling to the room temperature. The L value was also higher in PP-B (32 nm) than in PP-A (30 nm) at room temperature. The sharper scattering peaks in the profile of PP-B indicate that the lamellar packing in PP-B was more ordered than PP-A, which can be attributed to the better oriented shish–kebab structure formed initially. This again confirms that the precursor structure developed at the initial stage of flow-induced crystallization dictates the final morphology.

3.3.3. Azimuthal intensity profiles

The azimuthal angle, ϕ, is 0 or 180° along the equator and 90 or 270° along the meridian. For each ϕ, the average intensity at 2θ (= 12.6° ± 0.17°) of (110) reflection was extracted from the 2D WAXD patterns. Figs. 10 and 11 show the corresponding azimuthal intensity profiles for PP-A and PP-B, respectively. The azimuthal breadth, B_ϕ, was estimated from the full width at half maximum (FWHM) of the peak along equator. It is seen in these figures that the degree of orientation or B_ϕ reaches a steady state value rather quickly, about 5 min after cessation of shear. The much sharper peaks in PP-B than in PP-A indicate the higher crystal orientation in PP-B than in PP-A.

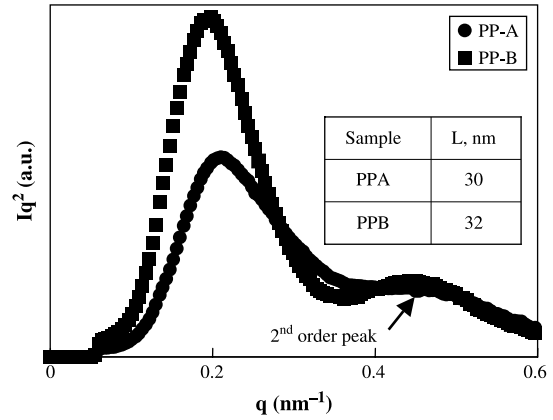

Fig. 9. Spacing between lamellae stacks at room temperature for PP-A and PP-B.

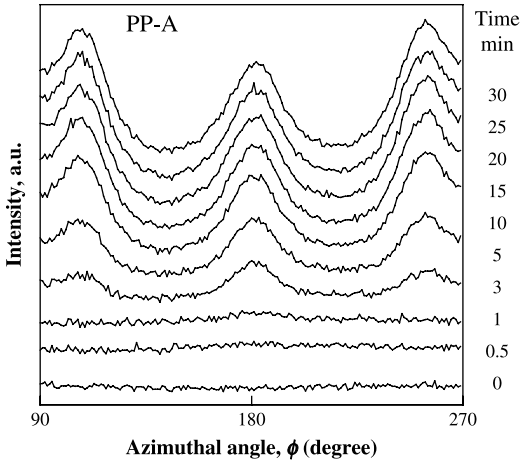

Fig. 10. Azimuthal intensity profiles at 2θ of (110) α reflection of *i*PP as a function of time after shear for PP-A (shear rate = 60 s^{-1}, duration = 5 s and T = 155 °C).

3.3.4. Oriented and unoriented crystals fraction

As mentioned above, diffraction intensity due to the oriented crystals is azimuthal dependent, while that due to the unoriented crystals (and amorphous phase) is azimuthal independent. Using the Halo method, contributions due to the oriented and unoriented crystals were obtained by deconvolution of Fraser-corrected 2D WAXD intensity patterns [38]. Circularly averaged WAXD intensity profiles were extracted from the 2D images for evaluation of the crystallinity index (representing the true crystallinity) due to the total (X_t), oriented (X_o) and unoriented (X_u) crystals. As an example, Fig. 12 shows the total intensity pattern (of PP-B at t = 30 min), and contributions due to the unoriented and oriented components. The average intensity profiles, extracted from the corresponding patterns, are also shown in this figure. A standard peak-fitting routine [33–34] was used to fit the

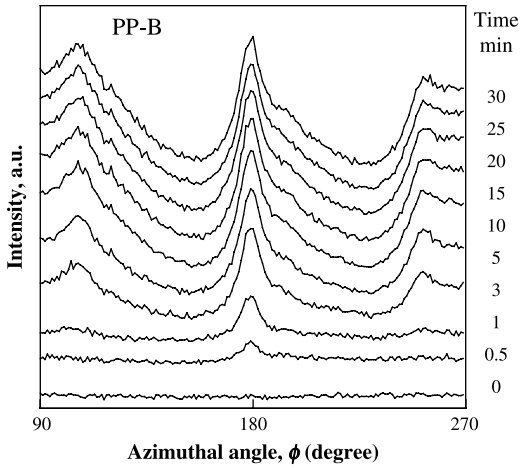

Fig. 11. Azimuthal intensity profiles at 2θ of (110) α reflection of *i*PP as a function of time after shear for PP-B (shear rate = 60 s^{-1}, duration = 5 s and T = 155 °C).

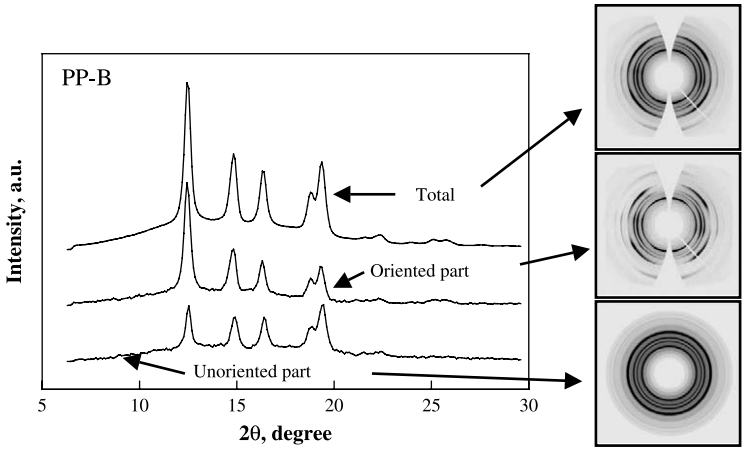

Fig. 12. Fraser corrected total WAXD intensity pattern of sheared PP-B sample and contributions due to oriented and unoriented part obtained after deconvolution by the Halo method [38]. The plot shows circularly averaged WAXD intensity profiles extracted from the total, oriented and unoriented parts.

crystalline peaks and amorphous phase halo in the intensity profiles. The normalized integrated intensity of each reflection (peak area) and amorphous background was obtained from the above fitting.

The total crystallinity index was determined after subtraction of the amorphous contribution in the total intensity profile. A_t, A_o and A_u represent the area sums of all diffraction peaks in the intensity profiles of total, oriented and unoriented crystals; respectively. The calculated values of the three area sums have the following relationship: $A_t = A_o + A_u$. This relationship was also confirmed by the addition rule of the three circularly averaged intensity profiles extracted from their corresponding 2D patterns (Fig. 12). The latter method provided an internal check for the accuracy of the image-image subtraction procedure using the Halo method [38]. The crystallinity index due to the oriented and unoriented crystals was obtained from the corresponding area sums, as follows:

$$\frac{X_o}{X_u} = \frac{A_o}{A_u} \tag{2}$$

$$X_t = X_o + X_u \tag{3}$$

Figs. 13 and 14 show the values of X_t, X_o and X_u as a function of time after shear for PP-A and PP-B, respectively. As expected, at early times after shear, X_t, X_o and X_u are higher for PP-B than PP-A. X_t, X_o and X_u increased with time and reached a plateau value for both samples, where the nature of these curves or the overall crystallization behavior appeared to be similar. It was seen later that, while the plateau values of X_t and X_u were higher for PP-B than PP-A, the plateau value of X_o was about the same for both polymers. This can be explained as follows: The quantity of oriented crystals formed was higher for PP-B than PP-A; however, since the quantity of the unoriented crystals was also higher, the calculated value of the ratio, X_o (= oriented crystals/total crystals), was about the same at the later stages. The half-time of crystallization, $t_{1/2}$, was used to characterize the overall crystallization kinetics. Fig. 15 shows the relative crystallinity index (total), which is $X_t(t)$ divided by its plateau value, for both samples. The half-time of crystallization was determined as the time when the relative crystallinity index reached the 0.5 value. It was about 8 min for PP-B compared to about 10.25 min for PP-A. Thus, the overall crystallization rate was higher for PP-B than PP-A.

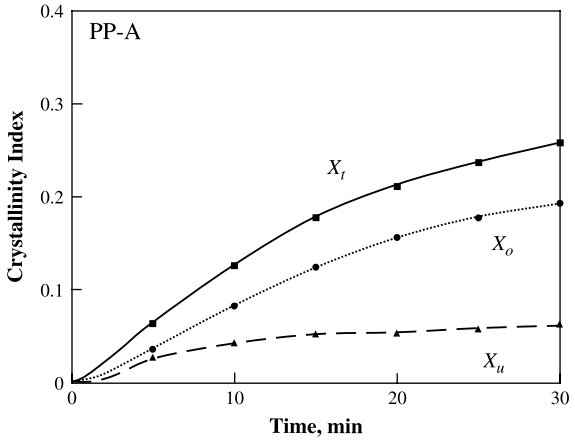

Fig. 13. The total crystallinity index, and contributions due to oriented and unoriented crystals (WAXD) as a function of time after shear for PP-A (shear rate = 60 s^{-1}, duration = 5 s and T = 155 °C).

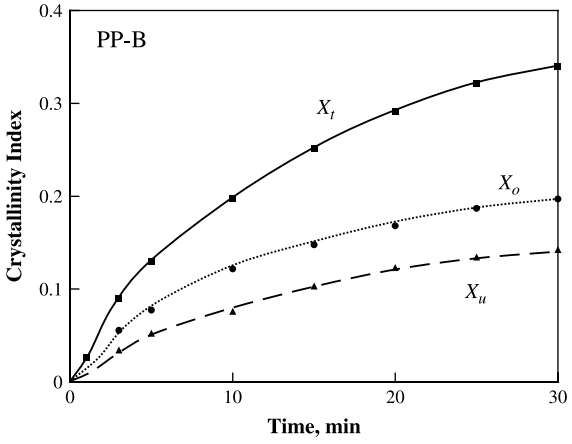

Fig. 14. The total crystallinity index, and contributions due to oriented and unoriented crystals (WAXD) as a function of time after shear for PP-B (shear rate = 60 s^{-1}, duration = 5 s and T = 155 °C).

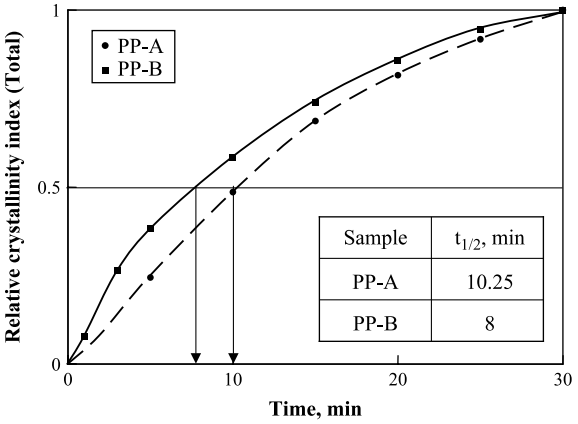

Fig. 15. Half-time of crystallization for PP-A and PP-B (shear rate $=60\,s^{-1}$, duration $=5$ s and $T=155$ °C).

4. Discussion

In situ rheo-SAXS and -WAXD results of the two *i*PP samples clearly showed that even a small increase in the amount of high molecular weight species (Fig. 1) enhanced the degree of crystal orientation (Figs. 10 and 11), and increased the oriented crystals fraction (Fig. 6) and crystallization rate (Fig. 15). Ideally, it is desired to image individual polymer chains as they reorganize to form crystals in real time. With current technology, observation of selective chains (particularly the high MW species) at the molecular level in polymer melts is difficult. It is generally believed, as evidenced by studies cited in the introduction section, that the basic mechanisms by which polymer chain length affects polymer crystallization kinetics and morphology is due to the extent of molecular orientation and/or stretching in flow as well as its relaxation behavior after cessation of flow. However, recently, different models for the role of the long chains were proposed. For example, Kornfield and coworkers [39] proposed that the primary mechanism, by which long chains enhanced the formation of row-nucleated structures, was the elaboration of point-like precursors into threads. It was claimed that the mechanism does not preferentially involve the most oriented chains or the long chains in the melt. The local stress or average level of segmental orientation was thought to be the dominant factor in determining the rate of formation of point-nuclei. The hypothesis that the addition of long chains would greatly enhance the formation of point-like nuclei following shear because of the stronger orientation of the longest molecules due to their long relaxation times was negated. On the other hand, Acierno, et al. [30] found that in shear, the transition to rod-like crystalline structure took place upon increasing the molecular weight. They concluded that the oriented long chains must be involved in the formation of shish. Our results concur with this scenario. Indeed, the local stress will govern segmental orientation as well as chain stretch. How to determine the differences in the local stress experienced by the short and long chains in flow and its relaxation after cessation of flow is not clear. In this regard, we believe that our experimental results provide new insights into the nature of oriented microstructures as they evolve in the sheared melt, especially because of the high sensitivity of in situ rheo-SAXS and -WAXD techniques. To help us understand the role of long chains at the molecular level, we follow the well-established Doi-Edwards model of polymer chain motion in dilute solution studies of dynamics of chain conformation in flow by S. Chu et al. [40–43]. Specifically, we focus on how chain-length affects: (1) the forces governing chain motion or reptation and relaxation behavior, and (2) the dynamics of chain conformation in flow.

4.1. Chain reptation and relaxation behavior

The basic concepts of the Doi-Edwards model are as follows [44]. In this model, the tube represents the constraints exerted on a given chain by the surrounding ones, the axis of which deforms affinely with the continuum. The tube diameter is assumed to remain constant and approximated as the entanglement mesh size. The chain tension or recoil, F, is assumed to have a constant value of $3kT/a$, where kT is the thermal energy and a is the tube diameter. The stress tensor is calculated from the ensemble average $<FR>$, where R is the end-to-end vector of a chain segment. Since, F is a constant, stress is due to the flow-induced orientational anisotropy of chain segments. Relaxation of the chain conformation occurs through the 1D diffusion of the chain out of the old tube; a process called reptation by de Gennes [45]. The original model predicts that, for monodisperse polymer melts, reptation time, τ_D, scales as 3 power of M_w, which is very close to the experimental value of 3.4. Over the past two decades, many modifications have been proposed to bring original theory in accord with experiment. The concept of 'contour-length fluctuations' [46] (CLF) was introduced, which shortens the portion of the tube that remains occupied. In polydisperse systems, 'constraint-release' [47] (CR) due to motion of the surrounding chains, often termed as 'double reptation' [48–49], was incorporated. Both CLF and CR reduce the stress and contribute to additional relaxation; thereby decreasing τ_D with respect to the prediction of the original reptation theory. We note that even in the model incorporating both CLF and CR, the stress is assumed to arise only due to segmental orientation, and is invalid only for small and slow deformations or slow flows. In the nonlinear range, i.e. large and fast deformations or fast flows, 'chain stretch' (CS) and 'convective constraint release' [44,50] (CCR) mechanisms become operative, even dominant. CS occurs when the imposed flow time scale, reciprocal shear rate ($\dot{\gamma}^{-1}$) /elongational rate ($\dot{\varepsilon}^{-1}$) rate is less than the Rouse relaxation time, τ_R. Chain stretch increases the tension in the chain above the equilibrium value of $3\,kT/a$ and hence increases the stress. CCR takes place as soon as the flow time scale is smaller than the reptation or disengagement time, τ_D. Although CCR is an additional relaxation mechanism, it may work in the direction of increasing the stress, especially in shear flows [51]. It must be mentioned here that the assumption of constant tube diameter in the standard model has been challenged; it has been suggested that tube diameter and distance between entanglements should be affected by flow [52–53]. However, the systematic analysis is not yet available.

Nevertheless, the above discussion allows us to predict the effects of chain length or molecular weight on its motion in an entangled melt.

Thus, especially in fast flows like those used in our experiments, high molecular weight (or long) chains will exhibit not only a high degree of chain segment orientation but also probably increased chain stretch compared to that of low molecular weight chains. The recent experiments by McLeash et al. [54] provide some clues for the relaxation behavior of the flow-induced segmental orientation. They used a contraction device in which the macroscopic stress field and microscopic conformation of polymer molecules in flow was imaged optically and by small-angle neutron scattering. The scattering map revealed that the orientation at the length scale of the entire chain decays considerably more slowly than at the smaller entanglement length. To estimate the relative difference in the relaxation time of the long and short chains in the polypropylene samples of the present study, reptation time for the long chains, τ_L, was estimated from the z-average molecular weight, M_z (approximating average length of long chains in the distribution) and that for the short chains, τ_s, from the weight average molecular weight, M_w (approximating average length of chains in the surrounding matrix). Thus, the ratio τ_L/τ_s is 60 for PP-B polymer compared to about 32 for PP-A polymer. The results of in situ rheo-SAXS experiments clearly showed that equatorial streak or shish evolved immediately after shear ($t=0.5$ min) in PP-B (Fig. 2), while the corresponding pattern of PP-A did not show any equatorial scattering. The only difference in the two samples is that PP-B has higher amount high M_w species compared to that in PP-A. The shorter time of evolution of shish in PP-B is a direct evidence that it must have originated from the aligned chain segments of the long chains in PP-B that are expected to exhibit higher orientation in flow and, subsequently, longer relaxtion time after cessation of flow. The corresponding rheo-WAXD results (Fig. 4), which showed evolution of the oriented crystals immediately following shear in the patterns of PP-B, while no crystals were observed in the patterns of PP-A, provide further evidence for the above.

4.2. Dynamics of chain conformation in flow

We start with the first effect of the imposed flow on coiled polymer chains. The coiled chain begins to deform when the force due to hydrodynamic friction across the molecule exceeds the entropic elasticity that tends to coil it. The amount of distortion in flow; with respect to the equilibrium and isotropic state, obviously, depends upon the flow type and the intensity as well as the molecular characteristics. In addition, molecular interactions with the surrounding medium affect its behavior, both in flow and after cessation of flow. This is especially significant in the case of entangled polymer melts compared to dilute solutions. At present, there are no reported studies of the conformational dynamics of individual polymer molecules in an entangled melt; however, the dilute solutions studies could be used as a guide. In dilute solutions under extensional flow, formation of the shish–kebab structures is best explained by the concept of *coil-stretch* transition proposed by de Gennes [55]. Accordingly, in the coiled state interior, monomer units are hydrodynamically shielded from the full velocity field as a result of nearby portions of the same polymer chain. However, as the molecule stretches, the hydrodynamic force exerted by the surrounding fluid increases and is able to exert a stronger frictional grip. Using simple polymer kinetic theory, de Gennes predicted that a polymer chain followed an S-shaped diagram of chain extension versus deformation rate. In steady-flow, the chain adopts one of the two stable molecular conformations: a highly stretched state or a compacted coiled state. Recently, Muthukumar et al. [6] calculated free energy landscape for dilute polymer solution (with monodisperse chains) under extensional flow. Their simulation results showed two populations of conformations: stretched and coiled, where the stretched chains crystallize into shish and the coiled chains form lamellae that are subsequently adsorbed onto the shish forming the kebabs.

The concept of *coil-stretch* transition was experimentally verified by direct, visual observations of the conformational dynamics of individual, flexible DNA molecules (that can be considered to resemble a polymer chain) in dilute solutions using video fluorescence microscopy by S. Chu et al. [1,39–42]. Their results showed that, in pure elongational flow, the extension approached very rapidly to a value close to the full contour length of the chain at relatively low strain rates, consistent with the predictions of de Gennes. However, in steady-state shear, the mean fractional extension was found to approach an asymptotic value of only 0.4–0.5 even at high values of flow intensity. They observed a strong heterogeneity in the dynamics and conformations of individual chains in flow. The conformation changed continuously, and at various times dumbbell, half-dumbbell, kinked, folded or hairpin shapes were observed. The observed fluctuations in molecular extension were attributed in part to the wide spectrum of initial, equilibrium conformations of each molecule upon flow inception. In shear flow, the extension increased when the chain segments were aligned with the flow eigenvector. Eventually, Brownian motion 'kicks' the molecule out of this orientation. The molecules tumble, stretch and retract in a stochastic manner depending on the coupling of the hydrodynamic drag forces and the Brownian forces. Our recent in situ X-ray and ex situ SEM results showed formation of shish–kebab entity with multiple shish in a sheared polyethylene blend [56]. We take guidance from the above-mentioned experimental observations and theoretical predictions, and present below our thoughts on the events during deformation of an entangled melt and the role oriented long chains in the formation shish.

First, the extent of orientation and/or stretching of monomer segments or sections of a polymer chain, confined between the entanglement points, depends upon their initial equilibrium conformation. In an entangled melt of polymer chains, chain segments that are aligned with the flow eigenvector orient and/or stretch. Let us call the resulting parallel conformation of one segment as '‖ segment'. Each chain consists of many ‖ segments randomly located along its length. Note that, based

on the laws of probability; some ‖ segment's of one chain will be closer to each other, while the others will be far apart. As the ‖ segments are formed, the other segments near ‖ segment's that were previously shielded are now exposed to full flow field. Drawing analogy from the dilute solution studies, mentioned above, these segments or chain sections can unwind resulting in fast and abrupt *coil-stretch-like* transition of a certain length of the chain (probably on the order of persistent length). Assume that 'SL' represents stretched length associated with one '‖ segment'. Due to simultaneous unwinding of many ‖ segments, it is likely that several 'SL' combine to form a long stretched length (on the order of multiple persistent lengths). Thus, after deformation, the initial entangled 'mesh' formed by several polymer chains exhibits several sections consisting of stretched chain lengths aligned parallel to each other. On the other hand, the chain segments that are not aligned with the flow field do not substantially orient and/or stretch, resulting in sections remained in the coiled state.

If we assume that, after cessation of flow, the relaxation of segmental orientation in the stretched sections follows the double reptation model with CS and CCR, we expect that, for the two similar polymers like PP-A and PP-B, the stretched length or its molecular weight will have the strongest influence. Also, from simple probability theory, it may be estimated that the long chains should have a larger number of the stretched sections compared to those in the short chains. These stretched sections form shish that manifest as equatorial streaks in the SAXS patterns. The streaks evolved almost instantaneously after shear in PP-B; while, at the same time, no streaks were observed in PP-A (SAXS pattern at $t=0.5$ min, Fig. 1). These results clearly indicate that the detectable concentration of shish was formed in PP-B immediately after shear, while it could only be detected at the later times in PP-A. This can only be attributed to the higher amount of long chains or high Mw species in PP-B compared to PP-A. In addition, as one might expect, the crystallization rate was higher for PP-B than PP-A (Fig. 15). This is again due to higher concentration of primary linear nuclei or shish, which strengthens the above hypothesis. Furthermore, the oriented crystal fraction was higher for PP-B compared to PP-A [Fig. 6(b) (SAXS), and Figs. 13 and 14 (WAXD)]. Hence we conclude that even a small increase in the concentration of high molecular weight species causes a significant increase in the formation, stability and concentration of the flow-induced oriented microstructure, especially linear nuclei or shish, and the final polymer morphology.

On the molecular level, this may be because of the following mechaism. When a polymer melt, consisting of entangled chains of different lengths, is deformed, the chain segments that are aligned with the flow eigenvector would exhibit the abrupt *coil-stretch-like* transition, while the other segments could remain in the coiled state. Since, flow-induced orientation decays much more slowly for long chains than for short chains, oriented high molecular weight species play a prominent role in the formation of stretched sections with chain segments aligned parallel to each other or shish.

5. Conclusions

The in situ rheo-SAXS and -WAXD results of two *i*PP samples with similar M_n but different M_w clearly demonstrated the effects of high molecular weight species on its crystallization behavior under flow. The important concluding remarks of this study can be summarized as follows.

1. The *i*PP sample containing a larger amount of long chain species exhibited: (a) higher degree of crystal orientation, (b) higher amount of the oriented crystal fraction, and (c) faster crystallization kinetics (i.e. shorter value of $t_{1/2}$).
2. The shorter evolution time of shish, initiated from the bundle of aligned chain segments, in the *i*PP sample with a higher amount of high molecular weight species is a strong evidence to support the hypothesis that the long chains are responsible for the shish formation. This is because long chains have more sections that exhibit a higher degree of orientation and/or stretching and, subsequently, longer relaxation times after cessation of flow compared to the short chains, consistent with the predictions of the double reptation model of chain motion and dilute solution studies of the dynamics of chain conformation in flow.
3. The crystallization precursor structure (i.e. the landscape of the shish–kebab network) induced by flow at the initial stage of crystallization clearly define the final morphology of the sample at room temperature.

Acknowledgements

We acknowledge the assistance of Drs Igors Sics and Carlos Avila-Orta for the synchrotron SAXS and WAXD experimental setup. We also thank the helpful discussion with Dr Lizhi Liu of Dow Chemicals for the preparation of this work. The financial support of this work was provided by NSF (DMR-0405432).

References

[1] Schroeder CM, Babcock HP, Shaqfeh ESG, Chu S. Science 2003;301:1515.
[2] Wunderlich B. In: Macromolular physics, Vol. 2. New York: Academic; 1973. p. 2.
[3] Strobl G. Eur Polym J 2000;E3:165.
[4] Lotz B. Eur Polym J 2000;E3:185.
[5] Gee RH, Fried LE. J Chem Phys 2003;118:3827.
[6] Dukovski I, Muthukumar M. J Chem Phys 2003;118:6648.
[7] Somani RH, Yang L, Hsiao BS, Agarwal P, Fruitwala H, Tsou AH. Macromolecules 2002;35:9096.
[8] Somani, RH, Nogales, A, Srinivas, S, Fruitwala, H, Tsou, AH, Hsiao, BS. Proceed. Int. Conf. on Flow Induced Crystallization of Polymers, 2001, 21.
[9] Somani RH, Yang L, Hsiao BS. Physica A 2002;304:145.
[10] Wang ZG, Hsiao BS, Sirota E, Agarwal P, Srinivas S. Macromolecules 2000;33:978.
[11] Li L, Jeu WH. Phys Rev Lett 2004;92:075506.
[12] Li L, Jeu WH. Macromolecules 2003;36:4862.
[13] Keller A, Kolnaar HW. Mater Sci Technol 1997;18:189.
[14] Keller A, Cheng SZD. Polymer 1998;39:4461.

[15] Eder G, Janeschitz-Kriegl H. Mater Sci Technol 1997;18:268.
[16] Liedauer S, Eder G, Janeschitz-Kriegl H, Jerschow P, Geymayer W, Ingolic E. Int Polym Proc 1993;8(3):236.
[17] Pogodina NV, Lavrenko VP, Winter HH, Srinivas S. Polymer 2001;42: 9031.
[18] Pogodina NV, Siddiquee SK, Egmond JW, Winter HH. Macromolecules 1999;32:1167.
[19] Pogodina NV, Winter HH. Macromolecules 1998;31(23):8164.
[20] Kumaraswamy G, Kornfield JA, Yeh F, Hsiao BS. Macromolecules 2002; 35:1762.
[21] Mathieu C, Thierry A, Wittmann JC, Lotz B. Polymer 2000;41:7241.
[22] Ryan AJ, Terrill NJ, Fairclough JPA. In: Cebe P, Hsiao BS, Lohse DJ, editors. Scattering of polymers. ACS Symp. Ser. 739. Washington DC: Oxford; 2000. p. 201.
[23] Ziabicki A, Alfonso GC. Macromol Symp 2002;185:211.
[24] Garcia Gutierrez M-C, Alfonso GC, Riekel C, Azzurri F. Macromolecules 2004;37:478.
[25] Hu W, Frenkel D, Mathot VBF. Macromolecules 2003;36:8178.
[26] Haudin J, Duplay C, Monasse B, Costa JL. Macromol Symp 2002;185:119.
[27] Vleeshouwers S, Meijer HEH. Rheol Acta 1996;35:391.
[28] Jerschow P, Janeschitz-Kriegl H. Int Polym Proc 1997;12(1):72.
[29] Bove L, Nobile MR. Macromol Symp 2002;185:135.
[30] Acierno S, Palomba B, Winter HH, Grizzuti N. Rheol Acta 2003;42:243.
[31] Somani RH, Hsiao BS, Nogales A, Srinivas S, Tsou AH, Sics I, Balta-Calleja F. Macromolecules 2000;33:9385.
[32] Nogales A, Hsiao BS, Somani RH, Srinivas S, Tsou AH, Balta-Calleja F, et al. Polymer 2000;42:5247.
[33] Somani RH, Hsiao BS, Nogales A, Srinivas S, Tsou AH, Balta-Calleja F, et al. Macromolecules 2001;34:5902.
[34] Somani RH, Bruger C, Hsiao BS, Stein RS. Proc ACS Div Polym Mater: Sci Eng 2001;85:429.
[35] Agarwal PK, Somani RH, Weng W, Mehta A, Yang L, Ran S, et al. Macromolecules 2003;36:5226.
[36] Somani RH, Yang L, Hsiao BS, Fruitwala H. J Macromol Sci, Part B: Phys 2003;B42:515.
[37] Yang L, Somani RH, Sics I, Hsiao BS, Kolb R, Lohse D, et al. Macromolecules 2004;37(13):4845.
[38] Ran S, Zong X, Fang D, Hsiao BS, Chu B, Ross R. J Appl Cryst 2000;33: 1031.
[39] Seki M, Thurman DW, Oberhauser JP, Kornfield JA. Macromolecules 2002;35:2583.
[40] Perkins TT, Smith DE, Chu S. Science 1997;276:2016.
[41] Smith DE, Babcock HP, Chu S. Science 1998;281:1335.
[42] Smith DE, Babcock HP, Chu S. Science 1999;283:1724.
[43] Babcock HP, Teixeira RE, Hur JS, Shaqfeh ESG, Chu S. Macromolecules 2003;36:4544.
[44] Marrucci G, Ianniruberto G. Macromolecules 2004;37(10):3934.
[45] de Gennes PG. J Chem Phys 1971;55:572.
[46] Doi M. J Polym Sci, Polym Lett Ed 1981;19:265.
[47] Graessley WW. Adv Polym Sci 1982;47:67.
[48] des Cloizeaux J. J Europhys Lett 1988;5:437.
[49] Mead DW. J Rheol 1996;40:633.
[50] Marrucci GJ. Non-Newtonian Fluid Mech 1996;62:279.
[51] Ianniruberto G, Marrucci G. J Non-Newtonian Fluid Mech 1996;65: 241.
[52] Marrucci G, de Cindio B. J Rheol Acta 1980;32:1.
[53] Wagner MH, Rubio P, Bastian H. J Rheol 2001;45:1387.
[54] Bent J, Hutchings LR, Richards RW, Gough T, Spares R, Coates PD, et al. Science 2003;301:1691.
[55] de Gennes PG. J Chem Phys 1974;60:5030.
[56] Hsiao BS, Yang L, Somani RH, Avila-osta CA, Zhu L. Phys Rev Lett 2005; 94:117802.